J Solid State Electrochem (2006) 10: 597–603
DOI 10.1007/s10008-006-0132-0

ORIGINAL PAPER

G. Etchegoyen · T. Chartier · P. Del-Gallo

Oxygen permeation in $La_{0.6}Sr_{0.4}Fe_{0.9}Ga_{0.1}O_{3-\delta}$ dense membrane: effects of surface microstructure

Received: 9 January 2006 / Accepted: 19 January 2006 / Published online: 30 March 2006

Abstract The use of perovskite mixed ionic–electronic conducting membranes for industrial applications, such as oxygen dissociation from air and methane conversion into syngas, requires high oxygen permeation fluxes. In this regard, the improvement of the permeation rates through a $La_{0.6}Sr_{0.4}Fe_{0.9}Ga_{0.1}O_{3-\delta}$ (LSFG) membrane was performed by modifying the surface by controlling the average grain size of the perovskite material or by coating its surface with a thin layer of $La_{0.6}Sr_{0.4}Co_{0.8}Fe_{0.2}O_{3-\delta}$. In both cases, the permeation-limiting regime was determined and the oxygen surface coefficient k_s and diffusion coefficient D_v were evaluated. The low value of k_s was found to be the most critical parameter for the performance of these LSFG membranes.

Keywords Mixed ionic–electronic conductors · Oxygen permeation · Surface exchange · Membrane microstructure · Perovskites

G. Etchegoyen · T. Chartier (✉)
Laboratoire de Science des Procédés Céramiques
et Traitements de Surface (SPCTS),
UMR-CNRS 6638, ENSCI, 47-73 Av. Albert Thomas,
87065 Limoges, France
e-mail: t_chartier@ensci.fr
Tel.: +33-5-55452222
Fax: +33-5-55790998

P. Del-Gallo
AIR LIQUIDE, Centre de Recherche Claude-Delorme,
1 chemin de la Porte des Loges, BP 126,
78354 Jouy-en-Josas, France

Present address:
G. Etchegoyen
Centre de Transfert de Technologies Céramiques (CTTC),
Parc d'Ester, Rue Soyouz, BP 36823,
87068 Limoges, France

Introduction

Thin, dense, mixed ionic–electronic conducting (MIEC) membranes have received considerable attention for their potential use in high-temperature applications such as oxygen separation from air and partial oxidation of methane. MIEC membranes should be of great interest for the transformation of natural gas into synthesis gas (syngas) [1–7] that could be converted into transportable fuels via Fischer Tropsch or methanol synthesis processes [8, 9].

The development of such ceramic mixed–conducting membranes requires specific knowledge of the oxygen transport mechanisms that control the overall permeation flux. For most mixed–conducting materials, the oxygen flux is controlled by oxygen ion diffusion through the membrane bulk in good agreement with the Wagner theory. But for some MIEC materials, oxygen exchanges at the membrane surfaces present lower kinetics (limiting mechanism) and, consequently, result in losses in the overall oxygen permeation kinetics. However, the oxygen flux can be significantly improved by acting on the rate-determining step, for example, by decreasing the dense membrane thickness when the bulk diffusion is dominating [10–14] or by coating the membrane with a catalyst to enhance oxygen surface exchanges [15–18].

Perovskite materials in the system $La_{1-x}Sr_xFe_{1-y}Ga_yO_{3-\delta}$ are promising materials for membrane applications due to their good chemical and dimensional stability in reducing environment [19–21]. However, Ga-containing materials were found to be mainly controlled by surface exchange mechanisms [22].

In this respect, the aim of this study is to examine the potential of the $La_{0.6}Sr_{0.4}Fe_{0.9}Ga_{0.1}O_{3-\delta}$ composition (referenced as LSFG) as mixed–conducting material for catalytic membrane reactor applications and to study the impact of surface modification on oxygen permeation flux. The $La_{0.6}Sr_{0.4}Co_{0.8}Fe_{0.2}O_{3-\delta}$ composition (referenced as LSCF) was also used as a catalytic porous surface layer.

Theory

Several models were developed during the past years to describe the oxygen permeation in a planar membrane considering both the oxygen surface exchange and bulk diffusion kinetics [23–26]. The model proposed by Kim et al. [22, 27, 28] interprets the surface exchange limitation as a chemical potential drop across the interface of the membrane, as previously described by Bouwmeester [29, 30] (Fig. 1). Based on this model, for the following equations, we consider that the major oxygen transport takes place through the oxygen vacancies. The various oxygen surface exchange mechanisms can be depicted by the global reaction:

$$\frac{1}{2}\mathrm{O_2} + \mathrm{V_O} \Leftrightarrow \mathrm{O^{2-}} + 2h^+. \tag{1}$$

The net oxygen flux $i\mathrm{O_2}$ through the interface will depend on the chemical potential drop according to [28]:

$$i\mathrm{O_2} = k_s c_v \left(e^{\mu \mathrm{O_2}(g)/2RT} - e^{\mu \mathrm{O_2}/RT}\right), \tag{2}$$

where k_s is the surface exchange coefficient, c_v is the oxygen vacancy concentration in equilibrium with the gas at the considered surface of the membrane, T is the temperature, R is the gas constant, $\mu\mathrm{O_2}$ is the oxygen chemical potential in the solid and $\mu\mathrm{O_{2(g)}}$ is the oxygen chemical potential of the gas depending on oxygen partial gas pressure $p\mathrm{O_2}$ (in atmospheres) such as:

$$\mu\mathrm{O_{2(g)}} = RT \ln\left(p\mathrm{O_2}\right). \tag{3}$$

The oxygen flux through the membrane bulk $I\mathrm{O_2}$ can be expressed as:

$$I\mathrm{O_2} = -\frac{1}{4lRT}\int_{\mu\mathrm{O_2^I}}^{\mu\mathrm{O_2^{II}}} C_v D_v d\mu\mathrm{O_2}, \tag{4}$$

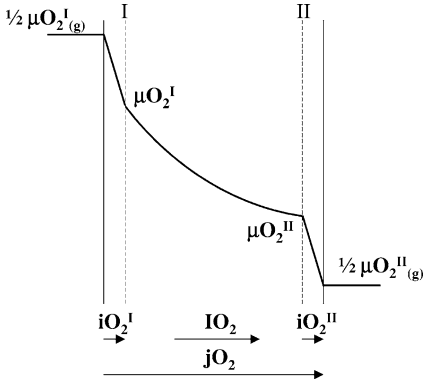

Fig. 1 Schematic representation of the chemical potential profile across a MIEC membrane

where D_v is the oxygen vacancy diffusion coefficient, C_v is the oxygen vacancy concentration in the membrane bulk, $\mu\mathrm{O_2^I}$ and $\mu\mathrm{O_2^{II}}$ are the oxygen chemical potential at the high and low pressure interfaces, respectively, and l is the thickness of the membrane.

Considering the continuity of the ion flux along all the membrane thickness, the overall ion permeation flux $j\mathrm{O_2}$ can be written in different forms:

$$\begin{aligned} j\mathrm{O_2} &= k_s c_v^I \left(e^{\mu \mathrm{O_2^I}(g)/2RT} - e^{\mu \mathrm{O_2^I}/RT}\right) \\ &= k_s c_v^{II} \left(e^{\mu \mathrm{O_2^{II}}/RT} - e^{\mu \mathrm{O_2^{II}}(g)/2RT}\right) \\ &= -\frac{1}{4lRT}\int_{\mu\mathrm{O_2^I}}^{\mu\mathrm{O_2^{II}}} C_v D_v d\mu\mathrm{O_2} \end{aligned}. \tag{5}$$

In a surface limited regime, the chemical potential drop at the surface is very important in comparison to the variation of $\mu\mathrm{O_2}$ in the membrane bulk, and thus, $\mu\mathrm{O_2^I} \rightarrow \mu\mathrm{O_2^{II}}$. The ion flux can then be written as [22]:

$$\begin{aligned} j\mathrm{O_2} &= \frac{1}{2}\left(i\mathrm{O_2^I} + i\mathrm{O_2^{II}}\right) \\ &= \frac{1}{2} k_s \frac{c_v^I c_v^{II}}{c_v^I + c_v^{II}} \left(\sqrt{p\mathrm{O_2^I}} - \sqrt{p\mathrm{O_2^{II}}}\right), \end{aligned} \tag{6}$$

where I and II exponents refer to the high and low-pressure interface, respectively. For it to be compared with literature data, the oxygen surface exchange coefficient (k_s^{o}) is usually normalized to air pressure ($p\mathrm{O_2}$=0.21 bar):

$$k_s^{\mathrm{o}} = k_s \sqrt{p\mathrm{O_2}}. \tag{7}$$

Considering that the oxygen diffusion coefficient D_v is approximately constant in the experimental conditions, as previously found for MIEC phases submitted to small oxygen pressure gradients [31], the permeation flux $j\mathrm{O_2}$ in a bulk diffusion regime where $\mu\mathrm{O_2} \rightarrow 1/2\mu\mathrm{O_{2(g)}}$ can be expressed by:

$$j\mathrm{O_2} = -\frac{D_v}{4l}\int_{\ln p\mathrm{O_2^I}}^{\ln p\mathrm{O_2^{II}}} C_v d\ln p\mathrm{O_2}. \tag{8}$$

Assuming that C_v and $\mu\mathrm{O_2}$ are following a linear variation between the two membrane surfaces, Eq. (7) can be rewritten as:

$$j\mathrm{O_2} = \frac{D_v}{4l}\frac{c_v^I + c_v^{II}}{2}\ln\frac{p\mathrm{O_2^I}}{p\mathrm{O_2^{II}}}. \tag{9}$$

Materials and methods

Materials synthesis

The details of the synthesis and characterization of materials were reported in previous papers [32, 33]. LSFG and LSCF powders were synthesized through a solid-state reaction. Appropriate amounts of precursors, i.e., La_2O_3 (99.99%, Ampère Industrie, France), Fe_2O_3 (99%, Sigma Aldrich Chemical), Ga_2O_3 (99.99%, Sigma Aldrich Chemical), Co_3O_4 (99%, Alfa Aesar), and $SrCO_3$ (99.9%, Sigma Aldrich Chemical), were weighed and roughly milled in a mortar. Mixtures were then attrition-milled in ethanol for 3 h using zirconia media. The obtained suspensions were dried and calcined in air at 1,100 °C for 10 h.

Powder characterizations

The resulting powders were characterized by X-ray diffraction using CuKα1 radiation on a Debye–Scherrer system and by inductively coupled plasma atomic emission spectrometer (Iris, Thermo Jarrel Ash). These analyses confirmed the formation of a single perovskite phase with the desired chemical composition. The oxygen content in the LSFG phase, equilibrated with air at room temperature, was evaluated by measuring the valence states and concentrations of iron ions by Mossbauer spectroscopy (^{57}Co and 4.2 K). To follow the variation of oxygen content with temperature, thermogravimetric analyses were performed at 2 °C/min from 20 to 1,000 °C in air and nitrogen atmospheres.

Membrane preparation

The elaboration of LSFG membranes was performed using a tape casting process. The LSFG powder was planetary milled for 3 h in the azeotropic mixture of butanone-2 and ethanol (60/40) with a dispersant (phosphate ester). For specific samples, various amounts of magnesia (2 and 5 vol%, grain size=0.5 μm) were added to the suspensions to control the sintered membrane microstructure as explained elsewhere [33, 34]. Then, an acrylic binder (methyl methacrylate, Degalan LP51/07, Degussa) and a phthalate plasticizer (dibutyl phthalate, Sigma Aldrich) were added to the slurries with a subsequent 10-h ball milling. The slurries were deaired for 2 days and tape-cast on a polymeric film using a doctor blade device. Green tapes with a thickness of 150 μm were punched to obtain 30-mm-diameter disks that were stacked and laminated under a pressure of 50 MPa at a temperature of 70 °C. Obtained green membranes were slowly debinded at 550 °C in air and sintered at 1,300 °C for 2 h in a 90% nitrogen/10% oxygen atmosphere.

Coated membranes were prepared by deposition of thin LSCF layers on both surfaces of LSFG using screen-printing. The slurry was composed of 35 vol% of LSCF powder, 63 vol% of resin (3% of ethylcellulose dissolved in terpineol) and 2 vol% of phosphate ester as a dispersant. Each membrane surface was coated with a surfacic weight of about 10 mg.cm^{-2}. After drying and firing at 1,000 °C for 1 h, both surfaces were covered by a 20-μm-thick, microporous LSCF layer showing good adhesion and no reaction with the dense LSFG material.

Oxygen permeation flux measurements

The oxygen permeation flux measurements were performed using a specific device described in detail in a previous publication [32]. Membranes were sealed with a Pyrex-based glass ring placed between the membrane and the alumina support tube. The disk edge was also coated by the sealant to minimize leakage. The bottom face of the membrane was exposed to an O_2/N_2 mixture with a flow rate of 200 ml(standard temperature and pressure).min^{-1}, while Ar was swept on the top face of the membrane with a similar flow-rate. A gas chromatograph (CP 3380, Varian) was used to control the membrane and seal tightness. For a gas-tight membrane, the oxygen content in argon flow was measured using a YSZ oxygen probe in the 800–925 °C temperature range.

Results and discussion

Oxygen nonstoichiometry

Figure 2 shows the dependence of the oxygen stoichiometry on temperature and gas nature (air or N_2) for LSFG. The stoichiometry dependence on T and pO_2 can be explained by the equilibrium between the different point defects in the crystal lattice.

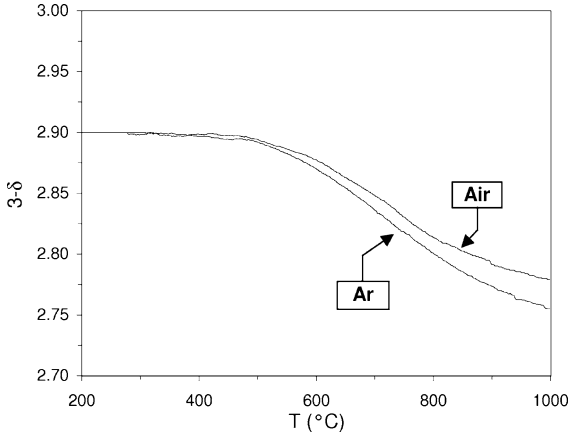

Fig. 2 Oxygen nonstoichiometry calculated from thermogravimetric data in argon and air flows

Using the Kröger–Vink notation, the dissolution of $SrFeO_3$ in $La(Fe,Ga)O_3$ perovskite structure can be described by:

$$SrFeO_3 \xrightarrow{La(Fe,Ga)O_3} Sr'_{La} + Fe^{\bullet}_{Fe} + 3O^{x}_{O}, \quad (10)$$

where the electronic charge excess, due to the substitution of La^{3+} by Sr^{2+}, is entirely compensated by the modification of the valence state of iron cations. However, it is well known that in MIEC perovskite materials, the charge compensation can occur via the formation of oxygen vacancies in competition with the precedent mechanism, resulting in the equilibrium:

$$2Fe^{\bullet}_{Fe} + O^{x}_{O} \Leftrightarrow 2Fe^{x}_{Fe} + V^{\bullet\bullet}_{O} + 1/2O_2(g). \quad (11)$$

This equilibrium, and so, the oxygen nonstoichiometry, is dependent on the oxygen gas pressure and temperature of the surrounding atmosphere, as can be seen on Fig. 2.

The variation of δ with temperature was obtained by measuring the mass variation of the powder on heating. However, the knowledge of the exact value of δ with T and pO_2 needs a reference value that can be indirectly determined by estimating the valence state of iron cations by Mossbauer spectrometry.

Due to the multivalent state of iron in the perovskite lattice, and in the absence of Fe^{2+} cations, the general formula of LSFG can be written: $La_{0.6}Sr_{0.4}Fe^{(+III)}_{0.9-x}Fe^{(+IV)}_{x}Ga_{0.1}O_{3-\delta}$, where the charge neutrality condition requires:

$$x + 2\delta = 0.4. \quad (12)$$

From Mossbauer spectra analysis, we deduce that x = 0.207 mol for the powder in equilibrium with air at room temperature, which enables us to give a reference state for the oxygen stoichiometry: $3 - \delta_{(25\,^{\circ}C,\,air)} = 2.90$.

Values of the vacancy concentration C_v were calculated from δ using:

$$C_v = \frac{\delta}{Vm}, \quad (13)$$

where Vm is the molar volume of the perovskite lattice: Vm=35.33 $cm^3.mol^{-1}$ for LSFG. The as-determined values of δ are necessary to calculate the right values of surface exchange coefficient k_s.

Table 1 Influence of the mean grain size controlled by magnesia addition on the normalized surface exchange coefficient

MgO content (vol%)	Mean grain size (μm)	k_s^o (850 °C, pO_2=0.21 bar) ($cm.s^{-1}$)
0	3.6	1.0×10^{-6}
2	1.8	7.6×10^{-6}
5	1.1	14.4×10^{-6}

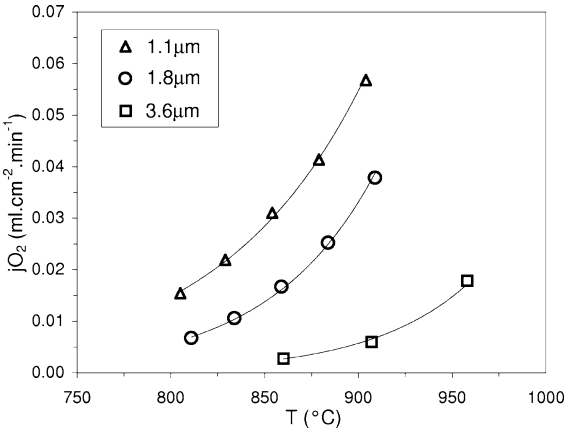

Fig. 3 Oxygen permeation flux of LSFG membranes with different average grain sizes

Permeation fluxes

Effect of the membrane microstructure

The LSFG membrane microstructure can be controlled with small amounts of magnesia inert rigid particles present at grain boundaries, acting as grain growth inhibitors [32]. In our sintering conditions (1,300 °C−2h−pO_2=10^{-2} MPa), the addition of MgO leads to a decrease of the LSFG average grain size from 3.6 μm (0 vol% of MgO) to 1.8 μm (2 vol% of MgO) or 1.1 μm (5 vol% of MgO).

Oxygen flux measurements on 1 mm-thick, dense, LSFG membranes are presented in Fig. 3 in a function of temperature and average grain size. The fluxes were found to be strongly dependent on the average grain size, increasing from 0.005 to 0.055 $ml.cm^{-2}.min^{-1}$ at 900 °C, as the mean grain size decreases from 3.6 to 1.1 μm. We previously demonstrated that no reactions occur between the LSFG phase and magnesia and that membrane densities remain the same whatever the magnesia volume content

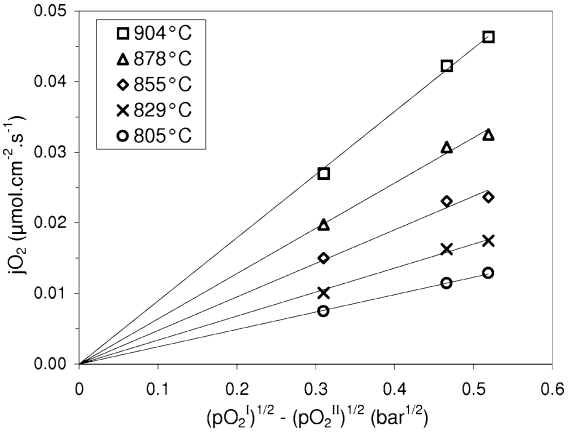

Fig. 4 Variation of the oxygen permeation flux of a LSFG membrane with an average grain size of 1.1 μm in function of $\left(pO_2^I\right)^{0.5} - \left(pO_2^{II}\right)^{0.5}$ for various temperatures

was in the range tested [33]. So, oxygen permeation flux was found to only depend on LSFG grain sizes.

A linear variation of the oxygen permeation flux vs $\sqrt{pO_2^I} - \sqrt{pO_2^{II}}$ for a 5-vol%, MgO-containing membrane was observed for each temperature between 805 and 904 °C in respect with Eq. (6) (Fig. 4), which clearly indicates a surface exchange regime in this temperature range. Similar behaviors were found for a 2-vol%, MgO-containing membrane and for a pure LSFG membrane. Normalized surface exchange coefficient values $\left(k_s^o\right)$ were calculated at 850 °C from line slopes in Fig. 4 and δ values from Fig. 2 using Eqs. (6), (7), and (13) for the different mean grain sizes (Table 1). The decrease of the average grain size of the sintered MIEC materials from 3.6 to 1.1 μm results in the increase of the surface exchange coefficient from 1.0 to 14.4×10^{-6} cm.s^{-1} and, consequently, in the improvement of the overall oxygen permeation flux.

Therefore, the surface microstructure seems to play an important role on the kinetics of surface reactions [Eq. (11)]. Although its exact role is not clear, the effect of the microstructure was thought to be caused by the difference of grain boundary density at the surfaces of the membranes. Indeed, the grain boundary density increases as the grain size decreases. Principal oxygen surface exchange elementary reactions, i.e., oxygen adsorption, charge transfer, or oxygen dissociation, may be enhanced at grain boundaries, thanks to high defect concentrations. Another explanation can be the modification of the electric field on the membrane surfaces with microstructural changes that can affect electrochemical reactions.

Even if the oxygen permeation rates were found to greatly increase with surface grain size reduction, surface exchange reactions were still limited for a 1.1-μm average grain size LSFG membrane.

Effect of membrane coating

The magnitude of oxygen permeation fluxes through 1-mm-thick LSFG membranes was greatly improved when a LSCF thin coated layer was used (Fig. 5). At 850 °C, the oxygen flux of the coated membrane with a fine microstructure (5 vol% MgO) reached 0.125 ml.cm^{-2}.min^{-1}, which is five times larger than the flux of the same uncoated membrane (Fig. 5b). Such an enhancement in the oxygen permeation flux was previously found by Lee et al. [16], who reported that the flux measured on a $La_{0.7}Sr_{0.3}Fe_{0.4}Ga_{0.6}O_{3-\delta}$ membrane at 950 °C can be increased by a factor of 6 if a porous layer of $La_{0.6}Sr_{0.4}CoO_{3-\delta}$ was used.

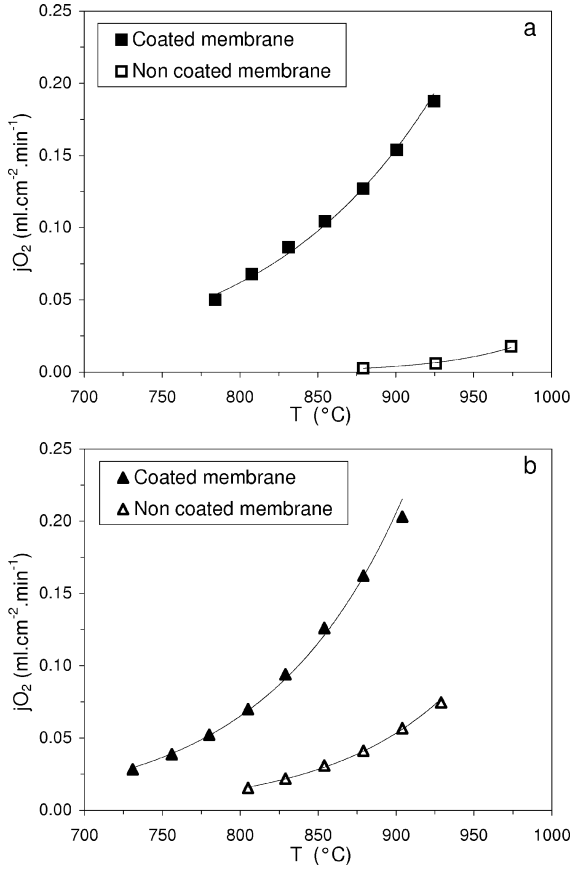

Fig. 5 Comparison of the oxygen permeation flux of uncoated and LSCF-coated membranes for LSFG membranes with a coarse-grain microstructure (3.6 μm) (**a**) and a fine-grain microstructure (1.1 μm) (**b**)

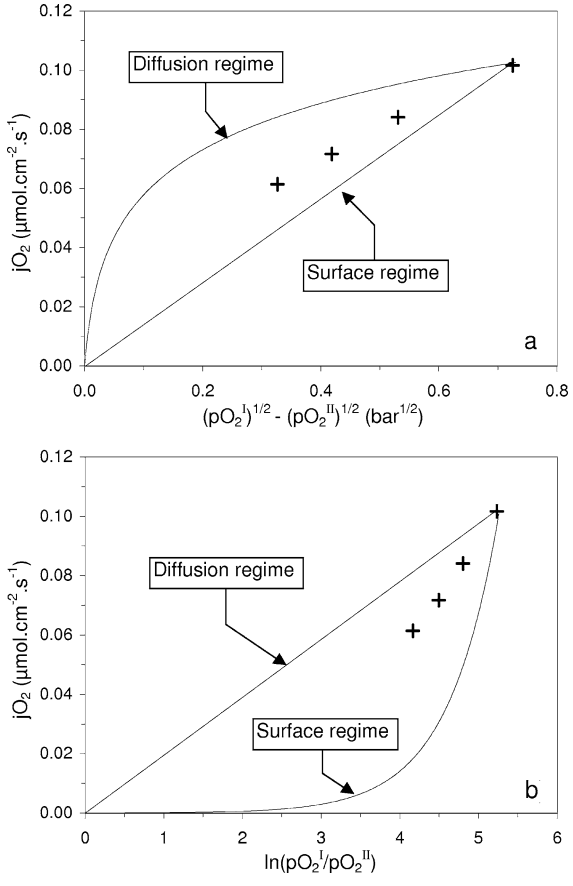

Fig. 6 Variation of the oxygen permeation flux of a coated membrane in function of $\left(pO_2^I\right)^{0.5} - \left(pO_2^{II}\right)^{0.5}$ (**a**) and $\ln\left(pO_2^I/pO_2^{II}\right)$ (**b**). Experimental data are represented by *crosses*. The *solid lines* were calculated using Eqs. 6 and 9

The comparison of the values of flux of coated membranes with fine (Fig. 5a) and coarse (Fig. 5b) bulk microstructures, i.e., mean grain sizes of 1.1 and 3.6 μm, respectively, does not show any significant difference, as previously observed on uncoated membranes. This result confirms that the grain size effect on permeation rates can be only attributed to surface phenomena in our experimental conditions. When the surface exchange reactions are shifted into the coated layer, the LSFG membrane microstructure seems to have no more influence on surface exchange kinetics.

Figure 6 reports the dependence of the oxygen permeation flux (jO_2) on pO_2^I and pO_2^{II} for a surface-modified membrane. As the variation of jO_2 in function of $\sqrt{pO_2^I} - \sqrt{pO_2^{II}}$ is not linear, the flux seems to be no longer controlled by the sole surface exchange reactions. The bulk diffusion regime described by Eq. (9) is no longer helpful to describe the overall permeation flux (Fig. 6b). These results suggest that the flux is governed by a mixed regime, for which bulk diffusion and surface exchange reactions both limit the oxygen transport.

Using Eq. (6) on Fig. 6a and Eq. (9) on Fig. 6b, in the explored oxygen partial pressure drop, the calculated values of $k_s \frac{c_V^I c_V^{II}}{c_V^I + c_V^{II}}$ are comprised of between 3.0×10^{-7} and 4.2×10^{-7} mol.cm^{-2}.s^{-1}.bar$^{-1/2}$, while the calculated values of D_v are in the interval 0.9×10^{-6}–1.2×10^{-6} cm^{-2}.s^{-1}. Assuming that the values of C_V^I and C_V^{II} are similar to those of an uncoated membrane, the mean value of k_s^o can be roughly estimated to 5.6×10^{-5} cm.s^{-1} at 850 °C. Even if the surface exchange coefficient can be significantly improved by coating the membrane with LSCF, its value is still low in comparison with other membrane materials [28, 35–37]. We have previously reported that the decrease of the thickness of the LSFG membranes was not efficient to significantly increase the oxygen flux of uncoated or coated membranes [32, 34]. It is obvious that the membrane surface exchange kinetics still have to be improved to reach the high oxygen permeation fluxes required for an industrial use.

Conclusion

A MIEC LSFG perovskite phase was synthesized and characterized to determine the oxygen nonstoechiometry or C_v dependence on temperature and oxygen partial pressure of the surrounding atmosphere. The knowledge of C_v enabled us to estimate the values of k_s^0 and D_v from oxygen permeation measurements.

The oxygen permeation fluxes through the LSFG membrane were found to be strongly dependent on the surface microstructure. The flux is controlled by a surface exchange mechanism in the tested temperature range with an oxygen exchange coefficient that significantly increases when the average grain size on membrane surface decreases. The surface was also modified by coating the membrane with a thin LSCF layer, improving oxygen permeation fluxes. For these coated LSFG membranes, the flux dependence vs pO_2 revealed a mixed regime for which surface exchange and bulk diffusion both determined the overall permeation kinetic.

The knowledge of the flux limitation mechanism was determinant to improving membrane performances, i.e., to increase k_s^0 and/or D_v, by controlling the microstructure of the different materials constituting the membrane and by tailoring the architecture of the membrane (multilayer assembly with gradients of composition and/or of porosity). These parameters will be considered in further studies to improve performances of LSFG-coated membrane performances, which were found to be mainly restricted by surface exchange.

References

1. Armor JN (1998) J Membr Sci 147:217
2. Dyer PN, Richards RE, Russek SL, Taylor DM (2000) Solid State Ion 134:21
3. Hazbun EA (1989) US Patent 4,827,071
4. Balachandran U, Dusek JT, Sweeney SM, Poeppel RB, Mieville RL, Maiya PS, Kleefisch MS, Pei S, Kobylinski TP, Udovich CA (1995) Am Ceram Soc Bull 74:71
5. Balachandran U, Ma B, Maiya PS, Mieville RL, Dusek JT, Picciolo JJ, Guan J, Dorris SE, Liu M (1998) Solid State Ion 108:363
6. Gottzmann CF, Prasad R, Schwartz JM (1999) European Patent 0,962,422,B1
7. Mazanec TJ, Cable TL (1997) US Patent 5,648,304
8. Stelmachowski M, Nowicki L (2003) Appl Energy 74:85
9. Lunsford JH (2000) Catal Today 63:165
10. Teraoka Y, Fukuda T, Miura N, Yamazoe N (1989) J Ceram Soc Jpn Int Ed 97:523
11. Chen CH, Bouwmeester HJM, van Doorn RHE, Kruidhof H, Burggraaf AJ (1997) Solid State Ion 98:7
12. Jin W, Li S, Huang P, Xu N, Shi J (2001) J Membr Sci 185:237
13. Hong L, Chen X, Cao Z (2001) J Eur Ceram Soc 21:2207
14. Middleton H, Diethelm S, Ihringer R, Larrain D, Sfeir J, Van Herle J (2004) J Eur Ceram Soc 24:1083
15. Lee KS, Lee S, Kim JW, Woo SK (2002) Desalination 147:439
16. Lee S, Lee KS, Woo SK, Kim JW, Ishihara T, Kim DK (2003) Solid State Ion 158:287
17. Kharton VV, Kovalevsky AV, Yaremchenko AA, Figueiredo FM, Naumovich EN, Shaulo AL, Marques FMB (2002) J Membr Sci 195:277
18. Teraoka Y, Honbe Y, Ishii J, Furukawa H, Moriguchi I (2002) Solid State Ion 152–153:681
19. Ishihara T, Tsuruta Y, Todaka T, Nishiguchi H, Takita Y (2002) Solid State Ion 152–153:709
20. Kharton VV, Shaulo AL, Viskup AP, Avdeev M, Yaremchenko AA, Patrakeev MV, Kurbakov AI, Naumovich EN, Marques FMB (2002) Solid State Ion 150:229
21. Ritchie JT, Richardson JT, Luss D (2001) AIChE J 47:2092
22. Kim S, Wang S, Chen X, Yang YL, Wu N, Ignatiev A, Jacobson AJ, Abeles B (2000) J Electrochem Soc 147:2398
23. Xu SJ, Thomson WJ (1999) Chem Eng Sci 54:3839
24. Lin Y-S, Wang W, Han J (1994) AIChE J 40:786
25. Lee TH, Yang YL, Jacobson AJ, Abeles B, Zhou M (1997) Solid State Ion 100:77

26. Gellings PJ, Bouwmeester HJM (1992) Catal Today 12:1
27. Kim S, Yang YL, Jacobson AJ, Abeles B (1999) Solid State Ion 121:31
28. Kim S, Yang YL, Jacobson AJ, Abeles B (1998) Solid State Ion 106:189
29. Bouwmeester HJM (2003) Catal Today 82:141
30. Bouwmeester HJM, Kruidhof H, Burggraaf AJ (1994) Solid State Ion 72:185
31. van Doorn RHE, Fullarton IC, de Souza RA, Kilner JA, Bouwmeester HJM, Burggraaf AJ (1997) Solid State Ion 96:1
32. Etchegoyen G, Chartier T, Del-Gallo P (2006) J Eur Ceram Soc (in press)
33. Etchegoyen G, Chartier T, Julian A, Del-Gallo P (2006) J Membr Sci 268:86
34. Etchegoyen G (2005) Ph.D. Thesis. Université de Limoges, Limoges
35. ten Elshof JE, Lankhorst MHR, Bouwmeester HJM (1997) Solid State Ion 99:15
36. ten Elshof JE, Bouwmeester HJM, Verweij H (1995) Solid State Ion 81:97
37. ten Elshof JE, Bouwmeester HJM, Verweij H (1996) Solid State Ion 89:81